SLAC-PUB-10331 Rev

May 2004

(A)

A systematic study of polarized electron emission from strained GaAs/GaAsP superlattice photocathodes*

T. Maruyama, D.-A. Luh, A. Brachmann, J. E. Clendenin, E. L. Garwin

S. Harvey, J. Jiang, R. E. Kirby, and C. Y. Prescott

Stanford Linear Accelerator Center, Menlo Park, California 94025

R. Prepost

Department of Physics, University of Wisconsin, Madison, Wisconsin 53706

A. M. Moy

SVT Associates, Inc., Eden Prairie, Minnesota 55344

Submitted to Applied Physics Letters

*This work was supported by Department of Energy Small Business Innovation Research Grant No. DE-FG02-01ER8332 and Contract Nos DE–AC03–76SF00515(SLAC) and DE-FG02-95ER40896(Wisconsin).

A systematic study of polarized electron emission from strained GaAs/GaAsP superlattice photocathodes

T. Maruyama, D.-A. Luh, A. Brachmann, J. E. Clendenin, E. L. Garwin,
S. Harvey, J. Jiang, R. E. Kirby, and C. Y. Prescott

Stanford Linear Accelerator Center,

Menlo Park, California 94025

R. Prepost

Department of Physics, University of Wisconsin, Madison, Wisconsin 53706

A. M. Moy

SVT Associates, Inc., Eden Prairie, Minnesota 55344

Abstract

Spin-polarized electron photoemission has been studied for $GaAs/GaAs_{1-x}P_x$ strained superlattice cathodes grown by gas-source molecular beam epitaxy. The superlattice structural parameters are systematically varied to optimize the photoemission characteristics. The heavy-hole and light-hole transitions are reproducibly observed in quantum efficiency spectra, enabling direct measurement of the band energies and the energy splitting. Electron-spin polarization as high as 86% with over 1% quantum efficiency has been observed.

Polarized electrons have been essential for high-energy parity-violating experiments and measurements of nucleon spin structure, and polarized electron beams will be required for all future linear colliders. Polarized electrons are readily produced by GaAs photocathode sources. When a circularly polarized laser beam tuned to the bandgap minimum is directed to the negative-electron-affinity (NEA) surface of a GaAs crystal, longitudinally polarized electrons are emitted into vacuum. The electron polarization is easily reversed by reversing the laser polarization. The theoretical maximum polarization of 50% for natural GaAs was first exceeded in 1991 using the lattice mismatch of a thin InGaAs layer epitaxially grown over a GaAs substrate to generate a strain in the former that broke the natural degeneracy between the heavy- and light-hole valence bands. [1] Polarizations as high as 78% were produced for the Stanford Linear Collider (SLC) from photocathodes based on a thin GaAs epilayer grown on GaAsP. [2], [3] However, after 10 years of experience with many cathode samples at several laboratories, [4], [5] the maximum polarization using the GaAs/GaAsP single strained-layer cathode remains limited to 80%, while the quantum efficiency (QE) for a 100-nm epilayer is only 0.3% or less. Two known factors limit the polarization of these cathodes: 1) a limited band splitting; and 2) a relaxation of the strain in the surface epilayer since the 10-nm critical thickness [6] for the 1% lattice-mismatch is exceeded. Strained superlattice structures, consisting of very thin quantum well layers alternating with lattice-mismatched barrier layers are excellent candidates for achieving higher polarization since they address these two issues. Due to the difference in the effective mass of the heavy- and light-holes, a superlattice exhibits a natural splitting of the valence band, which adds to the strain-induced splitting. In addition, each of the superlattice layers is thinner than the critical thickness. Polarized photoemission from strained InGaAs/GaAs [7], InGaAs/AlGaAs [8], and GaAs/GaAsP [9] [10] superlattice structures have been reported in the literature. However, the strained superlattice structure has many parameters, and a procedure for systematic optimization is lacking. This letter reports an investigation of strained GaAs/GaAsP superlattice samples in which the principal structural parameters are systematically varied to define the optimum structural details.

The samples were grown using gas-source molecular beam epitaxy (GSMBE). Group-V sources were As_2 and P_2 thermally cracked from AsH_3 and PH_3. High purity elemental Ga provided the Group-III source. A 0.2-μm-thick p-type GaAs buffer layer was grown on a (100) n-type GaAs substrate. In order to produce a strain-relieved $GaAs_{1-x}P_x$ layer on GaAs, a 2.5-μm-thick $GaAs_{1-y}P_y$ layer was grown with an increasing phosphorus fraction from $y = 0$ to x to accommodate the lattice mismatch, followed by an additional 2.5-μm-thick $GaAs_{1-x}P_x$ layer with a fixed phosphorus fraction. The superlattice structure was then grown on this layer. The phosphorus fraction in the superlattice barrier $GaAs_{1-x}P_x$ was the same as in the buffer $GaAs_{1-x}P_x$ layer so that the superlattice GaAs well layers were fully strained while the superlattice $GaAs_{1-x}P_x$ barrier layers were fully relaxed. The superlattice layers were doped with beryllium to a value of 5×10^{17} cm^{-3}. On top of the superlattice layers, a 5-nm-thick GaAs surface layer was grown with a Be doping concentration of 5×10^{19} cm^{-3}. Four parameters specify the superlattice structure: the GaAs well width, the $GaAs_{1-x}P_x$ barrier width, the phosphorus fraction, and the number of periods. Table 1 summarizes the eleven superlattice samples studied here. In addition to the superlattice samples, a 90-nm thick single strained-layer reference sample (90 nm $GaAs_{0.95}P_{0.05}$ on $GaAs_{0.66}P_{0.34}$) was grown for comparison using the same growth method.

The crystallographic structure was analyzed with a double-crystal x-ray diffractometer. Diffraction patterns of (004) symmetric reflection and asymmetric reciprocal-space-maps around the (224) reflection were recorded. The grown samples had the phosphorus fraction within δx =0.01 and the superlattice period within 0.4 nm of the values shown in Table 1. Assuming abrupt superlattice interfaces, x-ray simulation software [11] based on a dynamic x-ray diffraction theory was used to measure the strain in the superlattice well layers.

Electron polarization and QE were measured in the SLAC Cathode Test System (CTS) equipped with a load-lock for cathode introduction/removal and a compact medium-energy (20 kV) retarding-field Mott detector for polarization measurements. [12] When excited by linearly polarized light, strained photocathodes show an azimuthal anisotropy in the QE. The QE anisotropy is caused by an asymmetric strain relaxation along the two orthogonal

directions [110] and [1$\bar{1}$0]. [13] The measured QE anisotropy is a measure of the overall strain relaxation and can be used to gauge if strain relaxation is causing any depolarization. The QE anisotropy is measured at the excitation photon energy that yields a maximum polarization.

Figure 1 shows the polarization and QE as a function of the excitation photon energy for Sample 3 and the single strained-layer reference sample. The peak polarization is 86% for Sample 3 and 81% for the single strained-layer sample, while the QE at the peak polarization is 1.2% and 0.3%, respectively. The superlattice-cathode QE spectrum shows two distinct steps as expected from the density of states for the two dimensional structure, whereas the cathode-QE spectrum for the single strained-layer cathode, which has a three-dimensional density of states, follows a smooth $\sqrt{E - E_g}$ behavior at the band gap energy (E_g). [14] The first step corresponds to the heavy-hole (HH) band to the conduction band excitation, while the second step corresponds to the light-hole (LH) band to the conduction band excitation. While an observable energy splitting between the heavy- and light-hole bands is expected for superlattice structures, it has never been observed in QE spectra previously. By fitting with a step function, the band gap energies of the HH and LH bands relative to the conduction band are measured to be $E_{HH} = 1.58$ eV and $E_{LH} = 1.66$ eV, indicated by arrows in Figure 1. The energy splitting between the HH- and LH-bands is 82 meV. In the single strained-layer sample, the HH-LH splitting is not observed in the QE spectrum. An earlier photoluminescence study performed on single strained-layer samples measured an energy splitting of 55 meV, [13] indicating that the energy splitting of the superlattice structure is more than 25 meV larger than that of the single strained-layer structure. The measured QE anisotropy of the superlattice samples was only 1.5%, while that of the single strained-layer sample was 10%.

When the phosphorus fraction is varied, the lattice-mismatch between the well and the barrier changes, thus the superlattice strain can be varied. While a larger phosphorus fraction generates a larger strain and therefore a larger energy splitting between the HH and LH bands, the strain within a layer may relax. For Samples 1, 2, 3, and 4, the phosphorus

fraction was increased from 0.25 to 0.40 keeping the total superlattice thickness constant. Figure 2 shows the peak polarization and QE anisotropy as a function of the phosphorus fraction for constant total thickness. The measured HH-LH energy splitting is also shown in the figure. Although the HH-LH energy splitting increased from 60 meV to 89 meV, the peak polarization and the QE anisotropy did not change significantly at about 85% and 1.7%, respectively, indicating that this degree of energy splitting is sufficient to maximize the spin polarization.

Using samples with the same well (4 nm)/barrier (4 nm) thickness and phosphorus fraction (x=0.36), the total superlattice thickness was varied. Figure 3 shows the peak polarization and QE anisotropy as a function of the number of superlattice periods using Samples 3, 5, 6, 7, and 8. Also shown in Figure 3 is the strain relaxation in the superlattice GaAs well layers measured using x-ray diffraction. Although the well width is smaller than the critical thickness, increased superlattice periods will result in strain relaxation. As the strain relaxation steadily increases with the superlattice thickness, the peak polarization and QE anisotropy appear constant at 85.5%, and 1.5%, respectively, for less than 15 periods. At more than 20 periods, however, the peak polarization decreases and the QE anisotropy increases rapidly.

The QE and polarization spectra can be understood in terms of the superlattice band structure. In particular, the band structure is very sensitive to the well width. Using samples with the same barrier thickness (3 nm) and phosphorus fraction (x=0.36), the well thickness was varied while the number of periods was adjusted to keep the same total superlattice thickness. Figure 4 shows the spin polarization as a function of the excitation photon energy for Samples 9, 10, and 11. As the well thickness was increased, the polarization spectra shifted towards lower energy. The peak polarization was, however, independent of the well thickness. The HH energy relative to the conduction band was measured to be 1.61 eV, 1.57 eV, and 1.55 eV for Samples 9, 10 and 11 respectively, which compares favorably with energies of 1.64, 1.60 and 1.57 eV calculated using the transfer matrix method. [15] While the changes in the band structure differentially affected the polarization spectra for energies

above the polarization peak, the maximum polarization remained constant at about 86%, indicating that the valence-band splitting for this range of well thicknesses was sufficient.

In conclusion, we have investigated polarized photoemission from strained GaAs/GaAsP superlattice structures by systematically varying the superlattice parameters. The heavy- and light-hole excitations have been observed for the first time in the QE spectra, enabling direct measurements of the heavy- and light-hole energy bands. Spin polarization as high as 86% is reproducibly observed with the QE exceeding 1%. The superlattice structures presented here have superior polarization and QE compared to the single strained-layer structures of GaAs/GaAsP photocathodes.

This work was supported by Department of Energy Small Business Innovation Research Grant No. DE-FG02-01ER8332 and Contract Nos. DE-AC03-76SF00515 (SLAC), and DE-AC02-76ER00881 (UW).

REFERENCES

[1] T. Maruyama, E. L. Garwin, R. Prepost, G. H. Zapalac, J. S. Smith, and J. D. Walker, Phys. Rev. Lett. **66**, 2376 (1991).

[2] T. Nakanishi, H. Aoyagi, H. Horinaka, Y. Kamiya, T. Kato, S. Nakamura, T. Saka, and M. Tsubata, Phys. Lett. A **158**, 345 (1991).

[3] T. Maruyama, E. L. Garwin, R. Prepost, and G. H. Zapalac, Phys. Rev. B **46**, 4261 (1992).

[4] R. Alley, H. Aoyagi, J. Clendenin, J. Frisch, C. Garden, E. Hoyt, R. Kirby, L. Klaisner, A. Kulikov, R. Miller, G. Mulhollan, C. Prescott, P. Saez, D. Schultz, H. Tang, J. Turner, K. Witte, M. Woods, A.D. Yeremian, M. Zolotorev, Nucl. Instrum. Methods A **365**, 1 (1995).

[5] K. Aulenbacher, C. Nachtigall, H.G. Andresen, J. Bermuth, T. Dombo, P. Drescher, H. Euteneuer, H. Fischer, D. v. Harrach, P. Hartmann, J. Hoffmann, P. Jennewein, K.H. Kaiser, S. Koebis, H.J. Kreidel, J. Langbein, M. Petri, S. Pluetzer, E. Reichert, M. Schemies, H.-J. Schoepe, K.-H. Steffens, M. Steigerwald, H. Trautner, and T. Weis, Nucl. Instrum. Methods A **391**, 498 (1997).

[6] J.W. Matthews and A.E. Blakeslee, J. Crystal Growth, **27**, 118 (1974).

[7] T. Omori, Y. Kurihara, Y. Takeuchi, M. Yoshioka, T. Nakanishi, S. Okumi, M. Tsubata, M. Tawada, K. Togawa, Y. Tanimoto1, C. Takahashi, T. Baba and M. Mizuta, Jpn. J. Appl. Phys., **33**, 5676 (1994).

[8] Yu. Mamaev, A. Subashiev, Yu. Yashin, E. Reichert, P. Dresher, N. Faleev, P. Kop'ev, V. Ustinov, and A. Zhukov, Phys. Low-Dim. Struct. **10/11**, 1 (1995).

[9] T. Saka, T. Kato, T. Nakanishi, S. Okumi, K. Togawa, H. Horinaka, T. Matsuyama, and T. Baba, Surf. Sci. **454-456**, 1042 (2000).

[10] T. Nishitani, O. Watanabe, T. Nakanishi, S. Okumi, K. Togawa, C. Suzuki, F. Furuta, K. Wada, M. Yamamoto, J. Watanabe, S. Kurahashi, M. Miyamoto, H. Kobayakawa, Y. Takeda, T. Saka, K. Kato, A. K. Bakarov, A. S. Jaroshevich, H. E. Scheibler, A. I. Toropov, and A. S. Terekhov, *AIP Conf. Proc.*, **570**, 1021 (2001).

[11] RADS, Bede Scientific, Boulder CO.

[12] T. Maruyama, A. Brachmann, J.E. Clendenin, T. Desikan, E.L. Garwin, R.E. Kirby, D.-A. Luh, J. Turner, and R. Prepost, Nucl. Instrum. Methods A **492**, 199 (2002).

[13] R.A. Mair, R. Prepost, H. Tang, E.L. Garwin, T. Maruyama, and G. Mulhollan, Phys. Lett. A **212**, 231, (1996).

[14] S. L. Chuang, *Physics of Optoelectronic Devices*, (Wiley, New York, 1995) pp. 88-90.

[15] C. Y. P. Chao and S. L. Chuang, Phys. Rev. B **46**, 4110 (1992).

TABLES

TABLE I. Strained GaAs/$GaAs_{1-x}P_x$ superlattice samples.

Sample	GaAs Well (nm)	$GaAs_{1-x}P_x$ Barrier (nm)	x	No. of periods
1	4	4	0.25	12
2	4	4	0.30	12
3	4	4	0.36	12
4	4	4	0.40	12
5	4	4	0.36	9
6	4	4	0.36	15
7	4	4	0.36	20
8	4	4	0.36	30
9	3	3	0.36	16
10	4	3	0.36	14
11	5	3	0.36	12

FIGURES

FIG. 1. Polarization and QE as a function of excitation light energy for Sample 3 (solid circles for polarization, and solid curve for QE) and a single strained-layer sample (open circles for polarization and dashed curve for QE).

FIG. 2. Peak polarization (solid circles), QE anisotropy (open circles) and measured HH-LH energy splitting (triangles) as a function of the phosphorus fraction.

FIG. 3. Peak polarization (solid circles), QE anisotropy (open circles), and strain relaxation (triangles) as a function of the superlattice period.

FIG. 4. Polarization as a function of the excitation light energy for the three superlattice samples with a different well width; 3 nm (open circles), 4 nm (triangles), and 5 nm (solid circles).

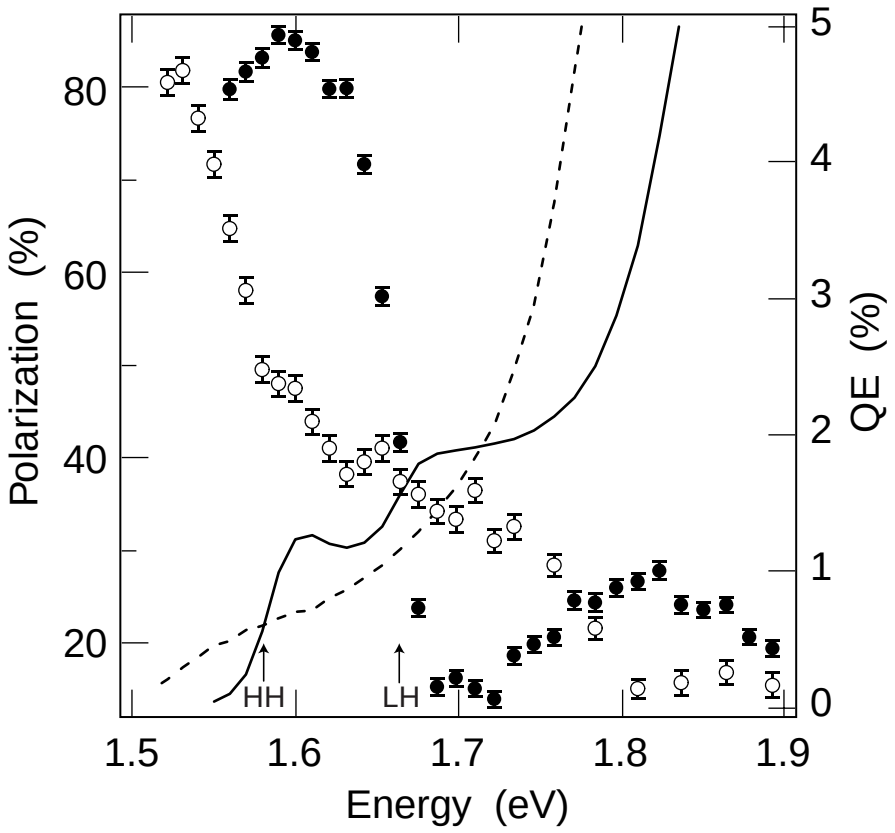
Polarization (%)
80
60
40
20
QE (%)
5
4
3
2
1
0
HH
LH
1.5
1.6
1.7
1.8
1.9
Energy (eV)

FIGURE 1

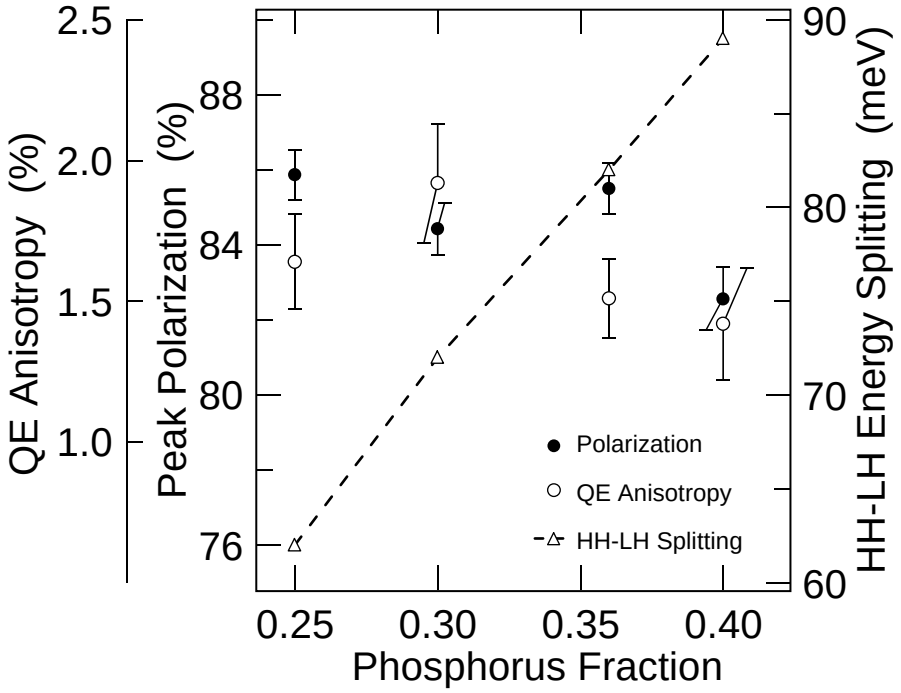
QE Anisotropy (%)
Peak Polarization (%)
HH-LH Energy Splitting (meV)
Phosphorus Fraction
2.5
2.0
1.5
1.0
88
84
80
76
90
80
70
60
0.25
0.30
0.35
0.40
Polarization
QE Anisotropy
HH-LH Splitting

FIGURE 2

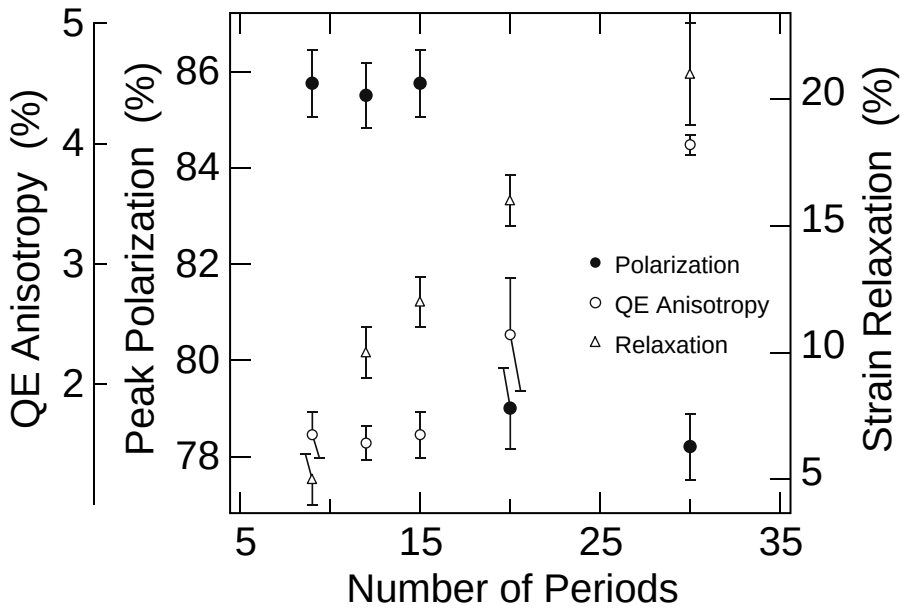
QE Anisotropy (%)
Peak Polarization (%)
Strain Relaxation (%)
Number of Periods
Polarization
QE Anisotropy
Relaxation
5
4
3
2
86
84
82
80
78
20
15
10
5
5
15
25
35

FIGURE 3

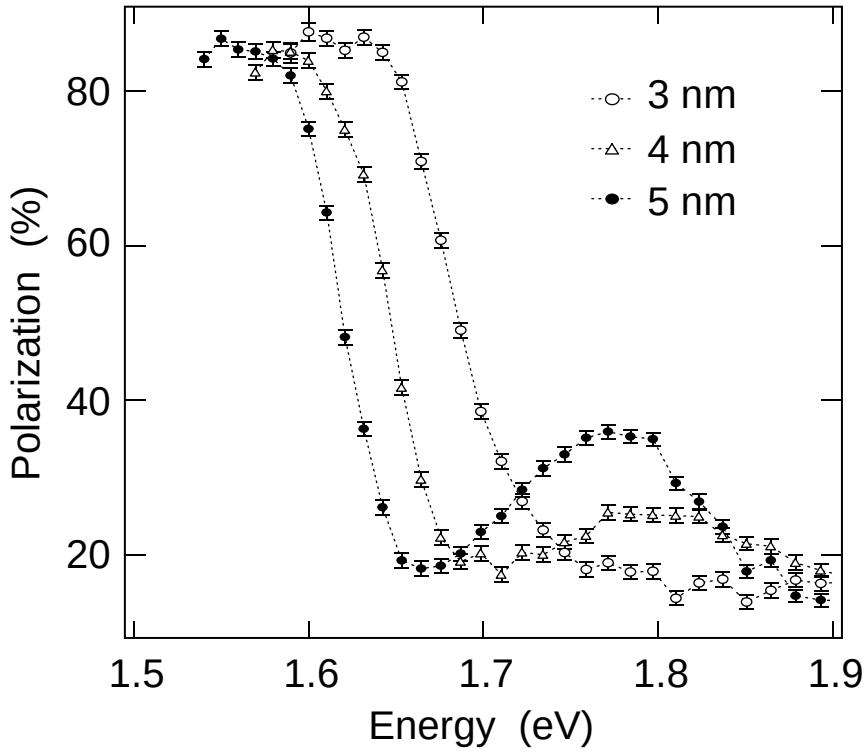

FIGURE 4